nature neuroscience

Regulation of neuronal morphology and function by the tumor suppressors Tsc1 and Tsc2

Sohail F Tavazoie[1,3,4], Veronica A Alvarez[1,4], Dennis A Ridenour[1], David J Kwiatkowski[2] & Bernardo L Sabatini[1]

Mutations in the *TSC1* or *TSC2* tumor suppressor genes lead to tuberous sclerosis complex (TSC), a dominant hamartomatous disorder that often presents with mental retardation, epilepsy and autism. The etiology of these neurological symptoms is unclear and the function of the TSC pathway in neurons is unknown. We found that in post-mitotic, hippocampal pyramidal neurons of mice and rats, loss of Tsc1 or Tsc2 triggered enlargement of somas and dendritic spines and altered the properties of glutamatergic synapses. Furthermore, loss of a single copy of the *Tsc1* gene was sufficient to perturb dendritic spine structure. Morphological changes required regulation of the actin-depolymerization factor cofilin at a conserved LIM-kinase phosphorylation site, the phosphorylation of which was increased by loss of Tsc2. Thus, the TSC pathway regulates growth and synapse function in neurons, and perturbations of neuronal structure and function are likely to contribute to the pathogenesis of the neurological symptoms of TSC.

TSC1 and *TSC2* are tumor suppressor genes whose protein products, hamartin (TSC1) and tuberin (TSC2), negatively regulate cell growth in a variety of systems. In humans, heterozygous mutations in either *TSC1* or *TSC2* lead to TSC, an autosomal-dominant hamartomatous disorder characterized by benign tumors in multiple organs including the brain, kidneys, heart and eyes[1]. TSC also typically presents with a constellation of neurological deficits that include epilepsy, mental retardation and autism.

Biochemical and genetic analyses in mammalian systems and *Drosophila melanogaster* have revealed that TSC1 and TSC2 participate in a conserved growth-regulating pathway involving the mammalian target of rapamycin (mTOR)[2–5]. In brief, the activation of growth-promoting receptor tyrosine kinases, such as the insulin receptor, stimulates phosphoinositide 3-kinase (PI3K) and the serine/threonine kinase Akt. *In vitro*, Akt phosphorylates TSC2 at conserved consensus phosphorylation sequences and downregulates its GTPase-activating protein (GAP) activity[6–8]. Reduced GAP activity allows the buildup of GTP-bound Rheb[9,10] and upregulates mTOR, which, through multiple actions, enhances protein translation and cell growth[11]. Thus, given the loss of heterozygosity of *TSC1* or *TSC2* found in hamaratomas of TSC patients[12], the growth of these benign tumors is thought to result from the increased mTOR activity and uncontrolled cell growth that accompanies interruption of the TSC pathway.

The pathogenesis of the neurological symptoms of TSC is unclear, and loss of heterozygosity is not seen within the brains of TSC patients[13]. The function of TSC1 and TSC2 in mammalian neurons and the defects that arise from hemizygosity of *TSC1* or *TSC2* are unknown. Many parallels exist, however, between the TSC pathway and those that link extracellular stimuli to synaptic refinement in neurons. For example, activation of the TrkB receptor tyrosine kinase by brain-derived neurotrophic factor (BDNF) stimulates PI3K and Akt to promote dendritic growth[14]. BDNF also triggers long-term potentiation of synaptic strength in an mTOR-dependent manner[15]. Similarly, strong activation of metabotropic glutamate receptors depresses synaptic transmission through a PI3K- and mTOR-dependent pathway[16,17].

Here we examine the role of the TSC pathway in regulating the growth of post-mitotic, differentiated neurons. We show that the TSC pathway regulates soma size, the density and size of dendritic spines, and the properties of excitatory synapses in hippocampal pyramidal neurons. These morphological effects are independent of regulation of Tsc2 by Akt at conserved phosphorylation sites but do require regulation of cofilin at a conserved LIM-kinase (LIMK) phosphorylation site. Furthermore, the TSC pathway is sensitive to gene-dosage effects, such that loss of a single copy of Tsc1, as is present in all neurons of TSC patients, is sufficient to perturb dendritic spine structure. Our results indicate that the TSC pathway regulates neuronal structure and function and suggest that the neurological symptoms of TSC are, at least in part, due to cell-autonomous perturbations of synapse function.

RESULTS

To uncover defects in neuronal structure and function caused by perturbation of the TSC pathway, we used transgenic mice carrying a conditional *Tsc1* allele (*Tsc1*^{C}) in which exons 17 and 18 are flanked by *lox*P sequences[18]. Loss of Tsc1 protein in neurons following transfection with a plasmid encoding a Cre recombinase–nuclear localization sequence fusion protein (Cre) was confirmed in dissociated hippocampal

[1]Department of Neurobiology, Harvard Medical School, 220 Longwood Avenue, Boston, Massachusetts 02115, USA. [2]Department of Medicine, Brigham and Women's Hospital, Harvard Medical School, 221 Longwood Avenue, Boston, Massachusetts 02115, USA. [3]Present address: Department of Medical Oncology/Hematology, Memorial Sloan-Kettering Cancer Center, 1275 York Avenue, New York, New York 10021, USA. [4]These authors contributed equally to this work. Correspondence should be addressed to B.L.S. (bsabatini@hms.harvard.edu).

Received 28 June; accepted 15 September; published online 6 November 2005; doi:10.1038/nn1566

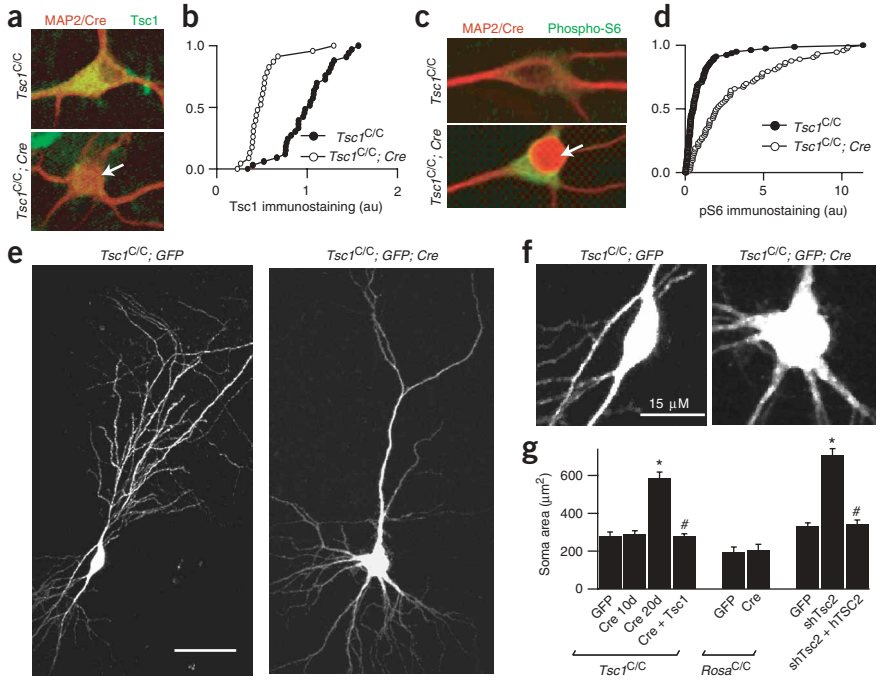

Figure 1 Cre expression in hippocampal neurons of *Tsc1*$^{C/C}$ mice leads to loss of Tsc1 protein, increased phosphorylation of S6 and increased soma size. (**a**) Untransfected (top) and Cre-transfected (bottom) neurons in a dissociated hippocampal culture from *Tsc1*$^{C/C}$ mice with immunoreactivity to MAP2 and Cre (red) and to Tsc1 (green). Arrow highlights red nucleus indicative of expression of the Cre-NLS fusion protein. (**b**) Cumulative distribution of Tsc1 immunostaining in Cre-transfected and untransfected neurons at 6 DPT. (**c**) Untransfected (top) and Cre-transfected (bottom) neurons with immunoreactivity to MAP2 and Cre (red) and to pS6 (green). Arrow highlights red nucleus indicative of expression of the Cre-NLS fusion protein. (**d**) Cumulative distribution of pS6 immunostaining in Cre-transfected and untransfected neurons at 6 DPT. (**e**) Images of GFP-transfected (left) and GFP/Cre cotransfected (right) pyramidal neurons in organotypic hippocampal slice from *Tsc1*$^{C/C}$ mice. Scale bar, 25 μm. (**f**) Enlarged views of the somas from neurons shown in **e**. (**g**) Summary of effects of loss of Tsc1 or Tsc2 on cross-sectional area of somas of hippocampal pyramidal neurons. Expression of Tsc1 or human TSC2 suppressed the effects of Tsc1 loss at 20 DPT and Tsc2 knockdown at 10 DPT, respectively. Expression of Cre in neurons from control ROSA26 locus (*Rosa*$^{C/C}$) mice had no affect on soma size. $^{*}P < 0.05$ compared to control, and $^{\#}P < 0.05$ for rescue experiments compared to perturbed phenotype (Cre- or shTsc2-expressing cells, as appropriate).

cultures prepared from mice homozygous for the conditional allele (*Tsc1*$^{C/C}$). Because transfection efficiency of neurons is low, we monitored Tsc1 levels by fluorescence immunohistochemistry (fIHC) (**Fig. 1a**,**b**). In neurons expressing Cre, cytoplasmic Tsc1 levels were significantly reduced at 6 days post-transfection (6 DPT) compared to untransfected neighboring neurons ($P < 0.05$, $n = 62$–67) (**Fig. 1b**). In several cell types, downregulation of TSC1/TSC2 upregulates mTOR activity and increases phosphorylation of the ribosomal protein S6[3,5,8]. Immunostaining against phosphorylated S6 (pS6) revealed a perinuclear cytoplasmic signal in neurons (**Fig. 1c**) that was abolished by application of rapamycin, a selective pharmacological inhibitor of mTOR (data not shown). PS6 levels were substantially higher in Cre-transfected *Tsc1*$^{C/C}$ neurons than in neighboring control neurons ($P < 0.05$, $n = 68$) (**Fig. 1c**,**d**). Thus, Cre transfection in post-mitotic, differentiated *Tsc1*$^{C/C}$ neurons induces recombination of the *Tsc1*^{C} allele, loss of Tsc1 protein and upregulation of mTOR.

Tsc1/2 regulate cell growth in differentiated neurons

Widespread loss of Tsc1 in the mouse brain, even when limited to astrocytes, leads to pronounced seizures[18], which may trigger changes in gene expression and synaptic transmission. To identify cell-autonomous neuronal defects caused directly by loss of Tsc1, we generated genetically mosaic brain tissue in which a small number of neurons lacking Tsc1 were located in otherwise normal brain tissue. This was accomplished by sparse transfection of pyramidal neurons with Cre and green fluorescent protein (GFP) in organotypic hippocampal slices prepared from *Tsc1*$^{C/C}$ mice.

GFP-transfected pyramidal hippocampal neurons were identified by their characteristic morphology (**Fig. 1e**) and location in a cell-dense band. Somas of Cre-transfected *Tsc1*$^{C/C}$ pyramidal neurons were larger than those of GFP-transfected neurons, reaching a roughly twofold enlargement at 20 DPT ($n = 20$–31, $P < 0.05$) (**Fig. 1e**–**g**). Changes in soma size were prevented by cotransfection with a plasmid encoding Tsc1 ($n = 8$). To control for nonspecific effects of Cre-mediated DNA recombination, similar measurements were made in tissue prepared from B6;129-*Gt(ROSA)26Sor*^{tm2Sho}/J mice that carry a floxed transcriptional stop upstream of the EGFP coding sequence in the Rosa26 locus (*Rosa*$^{C/C}$). Cre expression in *Rosa*$^{C/C}$ neurons had no effect on soma size ($n = 7$–8) (**Fig. 1g**), confirming that the increased soma size in *Tsc1*$^{C/C}$ neurons transfected with Cre was due to loss of Tsc1.

Soma size was also measured in rat neurons in which loss of Tsc2 was induced by RNA interference (RNAi; see Methods and **Fig. 1g**). Transfection of dissociated rat hippocampal pyramidal neurons with a dual-promoter plasmid encoding cytomegalovirus (CMV) promoter-driven GFP and a U6-driven short-hairpin RNA targeting *Tsc2* (shTsc2) reduced Tsc2 and increased pS6 (**Supplementary Fig. 1** online). In organotypic hippocampal slice cultures, somas of pyramidal neurons transfected with shTsc2 were enlarged relative to control neurons at 10 DPT ($n = 7$–13, $P < 0.05$) (**Fig. 1g**). This effect was occluded by cotransfection with human TSC2, which contains nine base pair changes within the region targeted by shTsc2 ($n = 9$) (**Fig. 1g**). Thus, soma size of post-mitotic, hippocampal pyramidal neurons is controlled by the TSC pathway. Somatic enlargement occurred with a shorter latency after shTsc2 transfection than after Cre transfection of *Tsc1*$^{C/C}$ neurons, likely reflecting the rapid degradation of mRNA triggered by RNAi.

Tsc1/2 regulate density and size of dendritic spines

In pyramidal neurons, the vast majority of excitatory synapses are made onto the heads of dendritic spines, and the morphology and density of dendritic spines reflect the properties and number of synapses. At 20 DPT, dendritic spines of *Tsc1*$^{C/C}$ neurons expressing GFP alone displayed roughly spherical spine heads separated from the dendrite by thin necks (**Fig. 2a**). In contrast, dendrites of *Tsc1*$^{C/C}$ neurons coexpressing Cre and GFP possessed elongated spines with greatly enlarged, bulbous heads. Quantification of these changes showed that Tsc1 loss increased spine length and head width and decreased the density of dendritic spines ($n = 9$–16 cells and

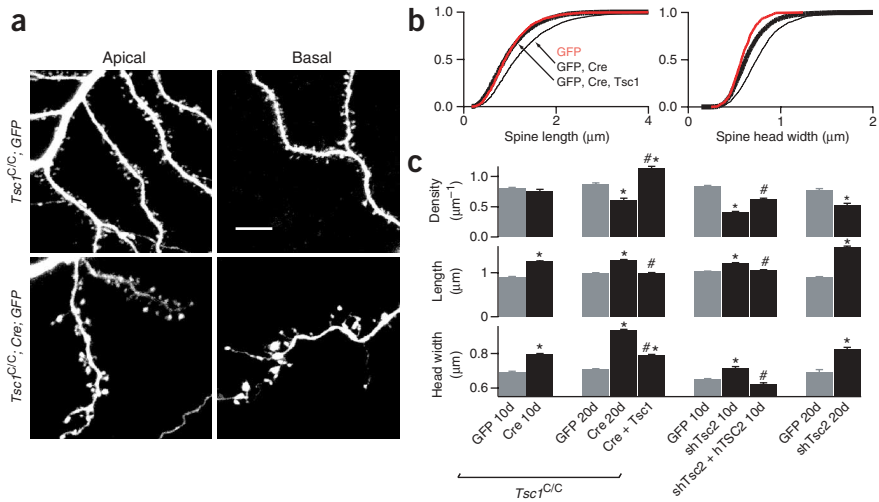

Figure 2 Loss of Tsc1 leads to increased size but decreased density of dendritic spines. (**a**) Images of apical (left) and basal (right) dendrites from *Tsc1*$^{C/C}$ pyramidal neurons in hippocampal organotypic slice culture. Neurons were transfected with GFP alone (top) or GFP and *Cre* (bottom). Scale bar, 10 μm. (**b**) Cumulative distribution of spine length and head width from *Tsc1*$^{C/C}$ neurons transfected with GFP alone; GFP and Cre; or GFP, Cre and Tsc1 at 20 DPT. (**c**) Summary of effects of Tsc1 or Tsc2 loss on dendritic spine density, length and head width. $^{*}P < 0.05$ compared to control neurons. $^{\#}P < 0.05$ for rescue experiments compared to perturbed phenotype (Cre- or shTsc2-expressing cells as appropriate).

2,441–4,344 spines, $P < 0.05$; **Fig. 2b,c**). Similar effects on spine size and morphology were seen at 10 DPT ($n = 7$–8 cells and 2,577–3,338 spines, $P < 0.05$; **Fig. 2**), a time point at which loss of Tsc1 has no effect on soma size (**Fig. 1g**). Changes in spine morphology and density were prevented by expression of *Tsc1* ($n = 8$ cells and 2,960 spines; **Fig. 2b,c**) and no changes in spine density or morphology were seen with Cre expression in *Rosa*$^{C/C}$ neurons (**Supplementary Table 1** online), confirming that the morphological changes seen with Cre expression in *Tsc1*$^{C/C}$ neurons were due to loss of Tsc1 protein.

The perturbations of spine morphology triggered by loss of Tsc1 were phenocopied by RNAi-mediated knock-down of Tsc2 in rat hippocampal neurons (**Fig. 2c**). Thus, at both 10 DPT ($n = 7$–13 cells and 1,715–5,023 spines) and 20 DPT (5–13 cells and 993–4,262 spines), dendritic spines of shTsc2-expressing neurons were elongated with enlarged spine heads ($P < 0.05$). These effects were rescued by expression of hTSC2 ($n = 9$ cells and 2,682 spines; **Fig. 2c**). Summaries of morphological parameters and numbers of cells and spines analyzed for each experimental condition are given in **Supplementary Table 1**.

Functional defects associated with loss of Tsc1

Do the enlarged spine heads seen after loss of Tsc1 contain functionally perturbed synapses? To address this question, we obtained whole-cell voltage-clamp recordings from *Tsc1*$^{C/C}$ pyramidal neurons transfected with Cre and from untransfected neighboring neurons. Spontaneous miniature excitatory postsynaptic currents (mEPSCs) were recorded (**Fig. 3a**). A red fluorophore was included in the recording pipette solution in order to fill the neuron and confirm its identity. At 10 DPT, mEPSC amplitude was roughly 20% higher in Cre-expressing neurons

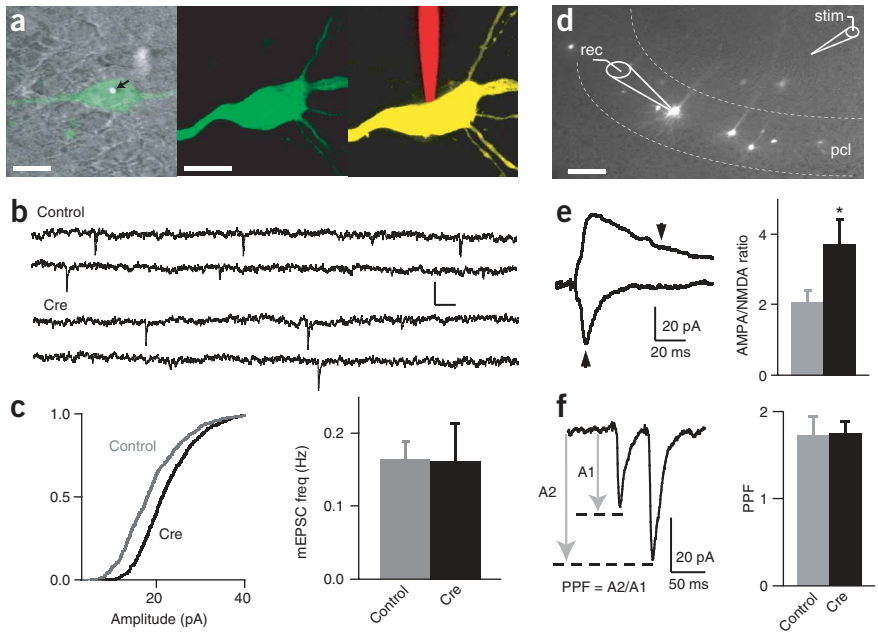

Figure 3 Loss of Tsc1 increases AMPAR-mediated synaptic currents. (**a**) Left, laser-scanning DIC image of the pyramidal cell layer of an organotypic slice culture from a *Tsc1*$^{C/C}$ mouse with superimposed green fluorescence from a GFP-expressing neuron. Note gold particle (arrow) in the nucleus of the transfected neuron. Image of a Cre/GFP-transfected pyramidal neuron before (middle) and after (right) filling with a red fluorophore through the whole-cell recording electrode. Scale bars, 15 μm. (**b**) Representative traces of mEPSCs recorded from control and Cre-transfected *Tsc1*$^{C/C}$ neurons. Scale bars: 20 pA, 200 ms. (**c**) Cumulative distributions showing increased mEPSC amplitudes in Cre-transfected (black trace) *Tsc1*$^{C/C}$ neurons compared to control neurons (gray trace) recorded at 10 DPT (left). Frequency of mEPSCs in untransfected and Cre-transfected *Tsc1*$^{C/C}$ pyramidal neurons at 10 DPT (right). (**d**) Wide-field image of a hippocampal organotypic slice culture from a *Tsc1*$^{C/C}$ mouse showing sparse GFP transfection of neurons in the pyramidal cell layer (pcl) and a schematic of relative positions of the recording electrode (rec) and stimulating electrode (stim) within the slice. Scale bar, 100 μm. (**e**) Evoked EPSCs recorded at –60mV (negative current) and +40mV (positive current) with arrowheads showing the times at which AMPAR (negative) and NMDAR (positive) mediated currents were measured (left). Mean AMPAR/NMDAR current ratios for control (gray bar) and Cre-transfected (black bar) *Tsc1*$^{C/C}$ neurons at 20 DPT (right). (**f**) Paired-pulse facilitation measured at a 50 ms interpulse interval in a Cre-transfected *Tsc1*$^{C/C}$ neuron at 20 DPT and summary data for control and Cre-transfected neurons. $^{*}P < 0.05$.

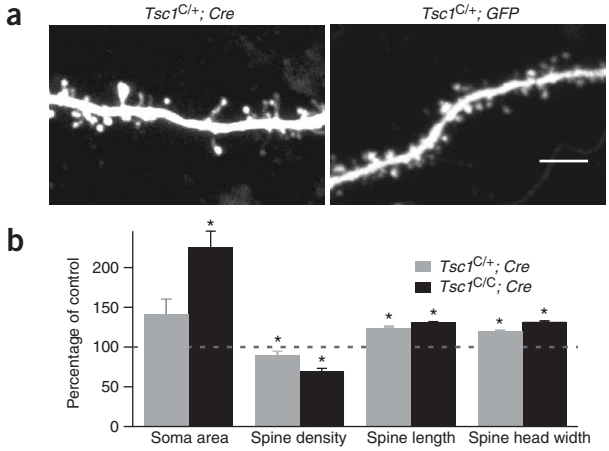

Figure 4 Neuronal morphology is sensitive to hemizygosity of *Tsc1*. (**a**) Dendrites of Cre/GFP (left) and GFP (right) transfected pyramidal neurons in hippocampal organotypic slice cultures prepared from $Tsc1^{C/+}$ mice at 20 DPT. Scale bar, 5 μm. (**b**) Relative soma cross-sectional area, spine density, length and head width for Cre-transfected $Tsc1^{C/+}$ and $Tsc1^{C/C}$ neurons compared to GFP-transfected neurons of each genotype. $^*P < 0.05$.

compared to neighboring control neurons (n = 10–12 cells and 660–781 events, $P < 0.05$; **Fig. 3b**,**c**), indicating an enhanced sensitivity to released neurotransmitter. No changes in mEPSC frequency (**Fig. 3c**) or in resting membrane resistance (R_{in}) and cell capacitance (C_m) were seen (controls: $R_{in} = 197 \pm 43$ MΩ, $C_m = 256 \pm 61$ pF; Cre-expressing neurons: $R_{in} = 200 \pm 63$ MΩ, $C_m = 182 \pm 34$ pF). In contrast, at 20 DPT, cells lacking Tsc1 had greatly reduced R_{in} (127 ± 15 MΩ vs. 185 ± 20 MΩ in control neurons, $P < 0.05$) and increased C_m (234 ± 24 pF vs. 171 ± 17 pF in control neurons) ($n = 13$ in each condition), making the comparison of mEPSCs between Tsc1-lacking neurons and control neurons difficult.

At 20 DPT, EPSCs evoked by stimulation of Schaffer collaterals (**Fig. 3d**) were monitored in CA1 pyramidal neurons at a holding potential of –60 mV, at which AMPARs are activated, and at +40 mV, at which the block of NMDA-type glutamate receptors (NMDARs) by Mg^{2+} is relieved and the long-lived NMDAR current is revealed (**Fig. 3e**). The ratio of evoked AMPAR- to NMDAR-mediated currents normally increases during development as well as after induction of long-term potentiation. In Cre-transfected neurons, the AMPAR/NMDAR current ratio was significantly increased relative to that in controls (3.7 ± 0.71 vs. 2.0 ± 0.35 in controls, $n = 13$ in each condition, $P < 0.05$), indicating an aberrant relative enhancement of synaptic AMPARs. To examine possible changes in presynaptic function induced retrogradely by postsynaptic loss of Tsc1, we recorded responses to a pair of stimuli and measured the paired-pulse facilitation (PPF). PPF was similar in untransfected and Cre-transfected neurons (1.73 ± 0.22 and 1.75 ± 0.15, respectively, $n = 11$–13; **Fig. 3f**), suggesting that release probability is not affected by postsynaptic loss of TSC1.

Figure 5 mTOR-dependent regulation of neuronal morphology. (**a**,**b**) Low-power images of the whole cell (left) and enlarged views of spiny dendrites (right) of (**a**) GFP- and (**b**) shTSC2-transfected pyramidal neurons in control media at 20 DPT (top) or for 14 d in control media followed by 6 d in 100 nM rapamycin (bottom). Scale bars, 30 μm (left) and 5 μm (right). (**c**) Summary of measured spine density, length, head size and soma area following application of rapamycin. Shaded areas indicate the mean ± 2 × s.e.m. of each parameter for control (dark gray) and shTsc2 (light gray) neurons determined in **Figures 1** and **2**. $^*P < 0.05$ compared to cells in control media.

Morphological effects of haploinsufficiency of Tsc1

Individuals afflicted with TSC carry heterozygous mutations in either the *TSC1* or *TSC2* genes and loss of heterozygosity, although present in hamartomas, is not seen within the brain. Therefore we tested whether loss of a single copy of Tsc1 is sufficient to trigger changes in neuronal morphology (**Fig. 4**). In tissue prepared from $Tsc1^{C/+}$ mice, Cre-expressing neurons had increased soma size, decreased spine density, increased spine length and increased spine head width relative to GFP-expressing neurons (n = 11 cells and 2,996 spines, $P < 0.05$). The morphological changes were less pronounced after loss of a single copy than after loss of both copies of *Tsc1* (**Fig. 4b**), suggesting that the TSC pathway is sensitive to gene dosage.

Regulation of neuronal morphology by mTOR

Rapamycin is a potent and specific inhibitor of mTOR, and is predicted to act downstream of TSC1 and TSC2. To determine whether the effects of loss of Tsc1 or Tsc2 on neuronal morphology are mediated by increased activity of mTOR, we examined the ability of rapamycin to reverse defects in neuronal morphology (**Fig. 5**). Neurons in hippocampal organotypic slices were transfected and maintained in culture for 14 d, a time point at which the effects of Cre-mediated loss of Tsc1 and RNAi-mediated loss of Tsc2 were apparent. Rapamycin (100 nM) was then added to the culture media, and the cultures were maintained for six more days before morphological analysis (total of 20 DPT).

Application of rapamycin to control GFP-expressing rat neurons had no effect on soma size but induced the growth of long, thin spines (n = 6 cells and 1,702 spines; **Fig. 5a**,**c**). Surprisingly, the mean length of dendritic spines on control cells in the presence of rapamycin was similar to that of Tsc2 knockdown cells (**Fig. 5a**,**c**). Unlike the phenotype resulting from loss of Tsc2, however, the rapamycin-induced spine phenotype did not show enlarged spine heads. Application of rapamycin to shTsc2-expressing cells reversed the enlargement of the soma and spine heads but further increased spine length (n = 8 cells and 1,163 spines, $P < 0.05$; **Fig. 5b**,**c**). In these cells, it was difficult to distinguish long filopodia and spines from nascent dendritic branches, artifactually lowering the measured spine density. Similar effects were seen in Cre-expressing $Tsc1^{C/C}$ cells, such that application of rapamycin

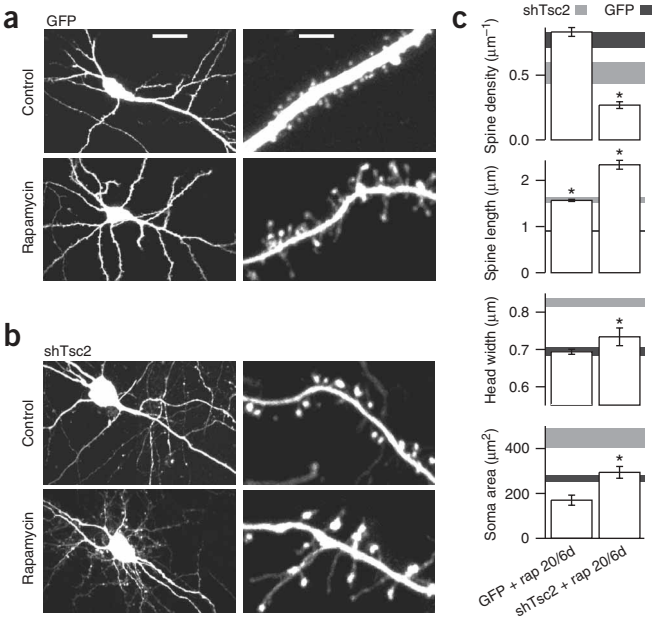

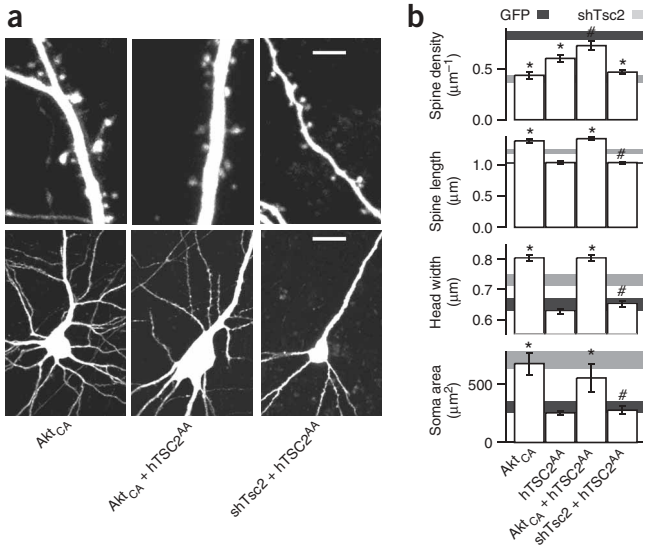

Figure 6 Akt upregulation phenocopies Tsc1/Tsc2 loss but does not require phosphorylation of Tsc2 at conserved Akt phosphorylation sites. (**a**) Images of pyramidal neurons (bottom) in organotypic slice cultures of rat hippocampus and enlarged views of spiny dendrites (top). Neurons were transfected with an Akt_{CA} (left); Akt_{CA} and $hTSC2^{AA}$ (middle); or shTsc2 and $hTSC2^{AA}$ (right) and imaged at 10 DPT. Scale bars, 5 μm (top) and 30 μm (bottom). (**b**) Summary of effects on spine density, length and head width. Shaded areas represent mean ± 2 × s.e.m. of each parameter for control (dark gray) and shTsc2 (light gray) neurons determined in **Figures 1** and **2**. $^{*}P < 0.05$ compared to control neurons. $^{\#}P < 0.05$ for $hTSC2^{AA}$ rescue experiments compared to shTsc2 or Akt_{CA} expressing neurons, as appropriate.

prevented the increase in soma and spine head sizes but further increased spine length (**Supplementary Table 1**). Thus, rapamycin-sensitive mTOR activity is epistatic to Tsc2 with respect to the regulation of soma and spine head sizes.

Epistatic analysis of Tsc2 and Akt

It has been proposed that Akt inhibits TSC2 by phosphorylation at two sites (S939 and T1462, numbered by the human sequence) that are conserved in *D. melanogaster* and mammals[7]. We investigated whether Akt regulates neuronal morphology and, if so, whether it occurs through phosphorylation of sites S939 and T1462 of Tsc2 (**Fig. 6**). Expression in rat hippocampal pyramidal neurons of a constitutively active Akt (Akt_{CA}), consisting of a myristoylated Akt lacking its pleckstrin homology domain (myrAktΔ4-129)[19], phenocopied loss of Tsc1/Tsc2, resulting in large somas, long spines and increased spine head size ($n = 5$ cells and 1,052 spines, $P < 0.05$; **Fig. 6a**,**b**). Three experiments were performed to determine if these effects are mediated by downregulation of Tsc2 by Akt through phosphorylation of S939 and T1462 (**Fig. 6** and **Supplementary Table 1**). First, $hTSC2^{AA}$ was expressed alone and found to have no effect on spine or somatic morphology ($n = 5$ cells and 1,014 spines). Second, expression of $hTSC2^{AA}$ did not occlude the changes triggered by overexpression of Akt_{CA} ($n = 5$ cells and 1,149 spines). Third, $hTSC2^{AA}$ expression in Tsc2 knockdown cells rescued spine and soma morphology with an efficiency equal to that of wild-type hTSC2 ($n = 5$ cells and 1,824 spines). Thus, phosphorylation of S939 and T1462 is not necessary for regulation of neuronal soma and spine size by Tsc2, and $hTSC2^{AA}$ is unable to act as a dominant negative with respect to the neuronal enlargement triggered by upregulation of Akt.

Morphological changes require signaling through cofilin

The mechanism by which the TSC pathway regulates neuronal morphology is unknown. Cofilin, a protein that depolymerizes and severs actin filaments and is widely expressed in the mammalian brain, has recently been shown to regulate spine size[20,21]. Cofilin is negatively regulated by LIMK through phosphorylation at a conserved site (serine 3). We examined whether phosphorylation at this site is regulated by the TSC pathway using fIHC to monitor levels of Ser3-phosphorylated cofilin (p-cofilin) in cultures of dissociated hippocampal neurons (**Fig. 7a**,**b**). At 10 DPT, shTsc2-transfected cells had higher p-cofilin levels than control neurons (**Fig. 7b**; $n = 34$–42 cells), whereas total cofilin levels were unchanged ($n = 26$–32 cells). In addition, p-cofilin, but not total cofilin, was increased in $Tsc2^{-/-}$ mouse embryonic fibroblasts (MEFs)[22] compared to $Tsc2^{+/+}$ MEFs ($n = 3$–5, $P < 0.05$; **Fig. 7c**,**d**). Similar results were obtained with a second commercial p-cofilin-specific antibody (see Methods, data not shown). Furthermore, the intensity of the ~19 kD band recognized by the p-cofilin antibody on western blots reflected levels of phosphorylated cofilin as its intensity was reduced in HEK293T cells transfected with the cofilin Ser3 phosphatase slingshot-1L[23]. No changes in intensity were noted following LIMK1 transfection, possibly reflecting additional regulation of the kinase activity independently of its expression level.

To determine whether increased cofilin phosphorylation is necessary for the spine enlargement described above, we expressed wild-type cofilin or cofilin with the LIMK phosphorylation site mutated to alanine (cofilin S3A) in shTsc2-transfected neurons in rat organotypic slice cultures (**Fig. 7e**). At 10 DPT, neurons expressing cofilin and shTsc2 had slightly reduced spine length compared to those expressing shTsc2 alone ($n = 9$ cells and 2,336 spines, $P < 0.05$) but similar soma size, spine head width and spine density. In contrast, expression of cofilin S3A in shTsc2-transfected neurons restored soma size, spine head width and spine density to control levels and decreased spine length to levels slightly below those of control neurons ($n = 6$ cells and 3,200 spines, $P < 0.05$ compared to shTsc2 neurons; **Fig. 7e**). Cofilin S3A expression in control neurons had no effect on soma size, spine head width and spine density, but it did reduce spine length ($n = 6$ cells and 4,243 spines, $P < 0.05$; **Fig. 7f**). The morphology of cofilin S3A/shTsc2-expressing cells was identical to that of cofilin S3A/GFP-expressing neurons (**Fig. 7g**), indicating that cofilin lies downstream of Tsc2 and that phosphorylation at Ser3 is necessary for the morphological changes induced by loss of Tsc2.

DISCUSSION

We have shown that the TSC pathway regulates the morphology and function of post-mitotic, hippocampal pyramidal neurons. Loss of Tsc1/Tsc2 triggered multiple changes in neuronal morphology, including increased soma and dendritic spine size as well as decreased dendritic spine density. These effects required both rapamycin-sensitive mTOR activity and regulation of cofilin at a conserved LIMK phosphorylation site. Furthermore, phosphorylation of cofilin, an actin-depolymerization factor not previously linked to the TSC pathway, was increased following loss of Tsc2. Synaptic strength and passive membrane properties were also altered in neurons lacking Tsc1, suggest that primary defects in neuronal function contribute to the neurological symptoms of TSC.

Relationship of Tsc2 and Akt

We found that expression of constitutively active Akt phenocopies the morphological defects seen with loss of Tsc1 or Tsc2. Increased Akt activity leads to enlarged neuronal size, in agreement with studies using overexpression of Akt or downregulation of PTEN, the lipid

phosphatase that antagonizes PI3K[6,24–27]. However, we found that the somatic and dendritic spine enlargement induced by increased Akt activity is independent of phosphorylation of TSC2 at S939 and T1462, the consensus sites conserved across *D. melanogaster*, rats, mice and humans. This is in contrast to findings in *D. melanogaster* in which expression of dTsc2$^{S924A/T1518A}$ suppresses the enlargement of ommatidia triggered by overexpression of Akt[6]. Furthermore, we found that expression of hTSC2^{AA} does not perturb spine or soma size and that it reverses the effects of loss of endogenous Tsc2. Again, these results are in contrast with the marked reduction in ommatidia size following dTsc2$^{S924A/T1518A}$ expression[6] but in agreement with recent findings that dTsc2$^{S924A/T1518A}$ is able to rescue the dTsc2-null phenotype in *D. melanogaster* development[28]. Lastly, our results are consistent with recent findings that indicate that Akt is regulated by mTOR[29] and thus lies downstream of Tsc1/Tsc2. In summary, our data indicate that, although upregulation of Akt and downregulation of Tsc1/Tsc2 result in similar phenotypes, phosphorylation of Tsc2 at S939 and T1462 is not necessary for the normal control of neuronal size or for the neuronal enlargement induced by upregulation of Akt.

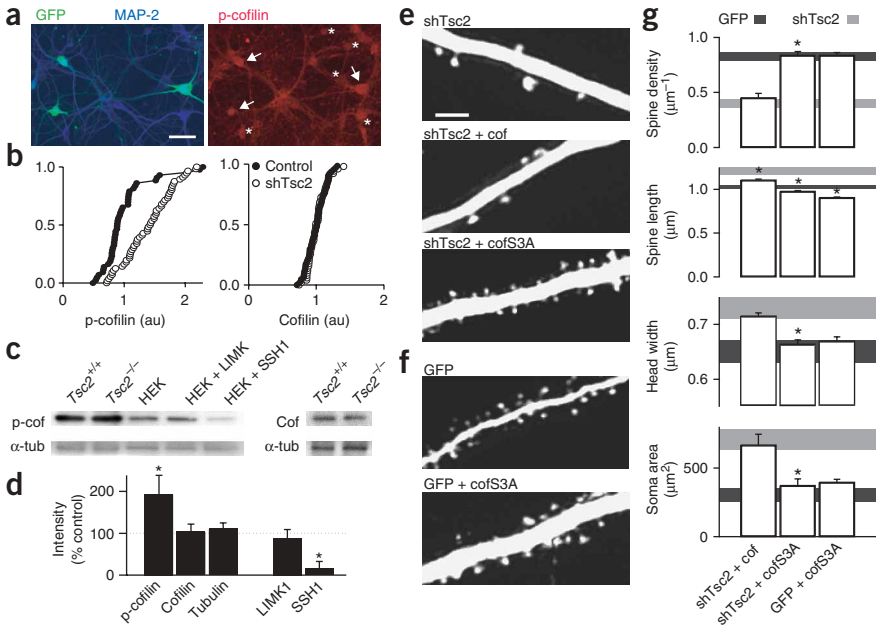

Figure 7 Phosphorylation of cofilin is regulated by Tsc2 and is necessary for increased cell growth. (**a**) Cultured hippocampal neurons transfected with shTsc2 showing GFP fluorescence (green, left), immunostaining for MAP2 (blue, left) and immunostaining for phosphorylated cofilin (p-cofilin) (red, right). Arrows and asterisks highlight shTsc2-transfected neurons and nontransfected neighbors, respectively. Scale bar, 20 μm. (**b**) Cumulative distribution of p-cofilin (left) and total cofilin (right) immunostaining in shTsc2-transfected and GFP-transfected neurons at 10 DPT. (**c**) Left, western blots of p-cofilin (left) from *Tsc2*$^{+/+}$ MEFs, *Tsc2*$^{-/-}$ MEFs, control HEK293T cells and HEK293T cells transfected with LIMK1 or slingshot-1L. Right, western blot of total cofilin in *Tsc2*$^{+/+}$ and *Tsc2*$^{-/-}$ MEFs. (**d**) Summary of band intensities for p-cofilin, cofilin and tubulin in *Tsc2*$^{-/-}$ MEFs relative to *Tsc2*$^{+/+}$ MEFs (left), and the intensities of p-cofilin bands in HEK cells transfected with LIMK1 or slingshot-1L relative to untransfected cells (right). $^*P < 0.05$. (**e**) Dendrites of pyramidal neurons in organotypic hippocampal slices transfected with shTsc2 (top), shTsc2+cofilin (middle) or shTsc2+cofilinS3A (bottom). Scale bar, 5 μm. (**f**) Dendrites of pyramidal neurons transfected with GFP (top) or GFP + cofilin S3A (bottom) imaged at 10 DPT. (**g**) Summary of the effects of the manipulations shown in **e** and **f** on spine density, length, head width and soma area. Shaded areas represent the mean ± 2×s.e.m. of each parameter for control (dark gray) and shTsc2 (light gray) neurons. $^*P < 0.05$ compared to neurons transfected with GFP or shTsc2 alone, as appropriate.

Molecular mechanisms of morphological perturbations

In addition to regulating mTOR activity, TSC1 and TSC2 are reported to participate in mTOR-independent signaling cascades that may regulate cell morphology. TSC1 interacts with and regulates the cytoskeleton via a C-terminal domain that binds ezrin-radixin-moesin (ERM) family proteins and an N-terminal domain that is capable of activating Rho GTPase in human endothelial cells[30]. TSC2 has been shown to activate Rho (in MDCK and ELT3 cells)[30], and increased Rho activity decreases spine length in hippocampal pyramidal neurons[31]. Furthermore, Rho GDP/GTP exchange factors (Rho-GEFs) regulate dendritic spine morphology and density[32,33]. TSC2 also interacts with 14-3-3 proteins[34,35], whose many cellular functions include trafficking of ion channels from the endoplasmic reticulum[36] and regulation of the actin cytoskeleton[37]. Importantly, TSC1 and TSC2 proteins stabilize each other[38], and thus reduced expression of either protein may induce a common set of morphological perturbations mediated through disruption of these mTOR-independent signaling cascades.

Which of these pathways is responsible for the changes in neuronal morphology observed here? Application of rapamycin to neurons with reduced Tsc1 or Tsc2 levels restores neuronal soma and dendritic spine head sizes to control levels, consistent with mTOR being downstream of Tsc1/Tsc2. In contrast, in the presence of rapamycin, spine morphology is clearly different in control neurons than in neurons with reduced Tsc1/Tsc2, arguing against a strictly epistatic relationship. Thus, Tsc1/Tsc2 may regulate soma and spine size via a rapamycin-sensitive mTOR-dependent pathway and spine length via a rapamycin-insensitive pathway. However, two caveats must be considered. First, long-term application of rapamycin may indirectly inhibit rapamycin-insensitive mTOR activity by sequestering mTOR and preventing formation of rictor-mTOR complexes[29,39]. Second, rapamycin may have mTOR-independent effects through the sequestration of FK506-binding proteins.

The central role of actin dynamics in determining spine structure strongly suggests that perturbed regulation of the actin cytoskeleton underlies the morphological changes described above. Indeed, we find a link between the TSC pathway and regulation of the cytoskeleton through cofilin. Cofilin is an actin depolymerization factor whose activity is downregulated following phosphorylation by LIM kinase at Ser3 (S3)[40]. Haploinsufficiency of LIMK1, a downstream effector of the Rho family of GTPases, results in the cognitive disorder Williams syndrome[41]. Both cofilin and LIMK1, as well as upstream regulators of the pathway such as PAK and Rho, have been shown to regulate dendritic spine morphology[21,42–45]. We found that phosphorylation of cofilin at S3 is necessary for the morphological changes triggered by loss of Tsc2, as they are occluded by expression of cofilin with this site eliminated (S3A). Our results also demonstrate that the balance of active and inactive cofilin is regulated by the TSC pathway in both neurons and MEFs, such that loss of Tsc2 leads to increased

S3-phosphorylated cofilin without changes in total cofilin. Possible mechanisms for this effect include mTOR-dependent translational control of a key regulatory protein as well as direct regulation of the enzymatic activity of PAK, LIMK1, or slingshot by mTOR or a downstream kinase such as Akt[29]. Alternatively, regulation of Rho through Tsc1-dependent protein-protein interactions[30] might mediate downstream regulation of cofilin.

Implication for tuberous sclerosis complex

Individuals with TSC show perturbations of cortical architecture including tubers, which are disorganized regions of the brain with disturbed lamination containing increased numbers of astrocytes and sparse neurons[1]. The correlation between the number of cortical tubers and the severity of seizure symptoms has led to the idea that the neurological deficits in TSC could arise from disruptions of cortical architecture[46]. Here we show that loss of a single copy of *Tsc1* results in defects in neuronal morphology, including increased soma size, decreased spine density and increased spine size. Therefore we propose that cell-autonomous neuronal defects due to haploinsufficiency of *TSC1* or *TSC2*, in addition to the perturbations of brain architecture caused by cortical tubers, subependymal nodules and giant cell astrocytomas, contribute to the pathogenesis of the neurological symptoms of TSC.

METHODS

Animals. We used mice carrying a conditional *Tsc1* allele[18] ($Tsc1^{C}$) consisting of *lox*P elements upstream of exon 17 and downstream of exon 18, as well as Sprague-Dawley rats (Charles River Laboratory). $Tsc1^{C/+}$ mice were generated by crossing $Tsc1^{C/C}$ mice with C57Bl6 mice (Charles River Laboratories). $Rosa^{C/C}$ mice (Jackson Laboratories) contain the EGFP coding sequence with an upstream *lox*P-flanked stop in the Gt(ROSA)26Sor locus. All animal procedures were conducted following Harvard Medical School guidelines. $Tsc1^{C}$ genotyping was performed using tail genomic DNA and primers F4536 (5′-ACGAGGCCTCTTCTGCTACC-3′) and R4830 (5′-CAGCTCCGACCAT GAAGT-3′), yielding 295-bp and 480-bp products from wild-type and conditional alleles, respectively.

Plasmids. All enzymes were obtained from New England Biolabs. The following plasmids were gifts: pBS::β-actin-nls-*cre* (S. Dymecki, Harvard Medical School); hTSC2 and $hTSC2^{AA}$ (E. Henske, Fox Chase Cancer Center, Philadelphia, Pennsylvania); pBS/U6 (Y. Shi, Harvard Medical School); cofilin and cofilinS3A (A. Minden, Columbia University); Slingshot1L and LIM-kinase1 (K. Mizuno, Tohoku University, Japan). pEGFP-N1 (Invitrogen) was used as a GFP control. For construction of the dual promoter CMV-EGFP/U6-shRNA vector, pEGFP-N1 was digested with *Bam*HI and *Bgl*II to remove the multiple cloning site (MCS) and designated as pEGFP-N1::ΔMCS. The U6 promoter and its downstream MCS from pBS/U6 were inserted into pEGFP-N1::ΔMCS at a filled-in *Afl*II site downstream of the SV40 polyadenylation sequence in the forward (pGUF) or reverse (pGUR) orientation relative to EGFP. Four sets of shRNAs directed against Tsc2 were designed from 19–21 bp coding sequences conserved in mice and rats with roughly 50% guanosines and cytidines ratio. Oligonucleotides containing the target sequence, a restriction site, the reverse complement of the target sequence, five threonine residues for U6 polymerase termination and an *Eco*RI site were synthesized (Integrated DNA Technologies). The shTsc2 clone used in this study was constructed from the following oligonucleotides: GGTGAAGAGAGCCGTATCACAAAGCTTTGTGATACGGC TCTCTTCACCCTTTTTG and AATTCAAAAAGGGTGAAGAGAGCCGTATC ACAAAGCTTTGTGATACGGCTCTCTTCACC. For production of shTsc2, pGUF was digested with *Apa*I, klenowed, digested with *Eco*RI and treated with calf intestinal alkaline phosphatase. Oligonucleotides were annealed, phosphorylated with T4 polynucleotide kinase and ligated into the digested pGUF to yield shTsc2.

Cultures and transfection. Dissociated hippocampal cultures were prepared from P3 rats and mice[47] and plated at 8×10^4 cells/well on glial monolayers on 12-mm glass coverslips. Cultures were transfected with Lipofectamine 2000 (Invitrogen) after 3–5 days *in vitro* (d.i.v.) in neuronal NEU media lacking biotin. Organotypic slice cultures were prepared from P5–P7 mice and rats[48] and biolistically transfected with a Helios Gene Gun (Biorad) after 2 d.i.v.. Bullets were prepared using 12.5 mg of 1.6 μm gold particles and 40–80 μg of plasmid DNA.

Immunofluorescence. Dissociated hippocampal neurons were fixed in 3.7% paraformaldehyde/4% sucrose for 15 min at 20–24 °C, permeabilized with 0.1% Triton X-100/PBS (Sigma) for 10 min, blocked with 1% goat serum/PBS (Jackson ImmunoLabs) and incubated with the following primary antibodies: anti-phospho-S6 ribosomal protein (1:100, Ser235/236; Cell Signaling), anti-MAP-2 (mouse, 1:500, Sigma), anti-MAP-2 (rabbit, 1:500, Chemicon), anti-Cre recombinase (mouse, 1:1,000, Chemicon), anti-Cre recombinase (rabbit, 1:1,000, Novagen), anti-p-cofilin1 (Ser3) (1:100, Santa Cruz) and anti-cofilin (1:200, Cell Signalling). Antibodies specific to tuberin and hamartin (1B2A8 and HF6, respectively) were kindly provided by V. Ramesh (Massachusetts General Hospital). The following secondary antibodies from Jackson Immunoresearch were used at a dilution of 1:500: Cy3-conjugated goat anti-rabbit, Cy3-conjugated goat anti-mouse, Cy5-conjugated goat anti-rabbit and Cy5-conjugated goat anti-mouse. Secondary antibody fluorescence was measured in transfected and untransfected neurons using an LSM510 confocal (Zeiss).

Western blotting. Lysates of $Tsc2^{-/-}$ and $Tsc2^{+/+}$ MEFs, and HEK293T cells (control or 24 h after transfection with LIMK1 or SSH1L), were separated by SDS-PAGE using 8–16% Tris-HCl gels (BioRad). Proteins were transferred onto a polyvinylidene difluoride membrane (PVDF, BioRad) overnight at 4 °C. Membranes were incubated in blocking solution (5% BSA, 0.1% Tween 20 in Tris-buffered saline) for 1 h at 20–24 °C, incubated overnight at 4 °C with primary antibodies (rabbit anti-p-cofilin S3 (1:200, Santa Cruz), rabbit anti-p-cofilin S3 (1:1,000, Cell Signalling), rabbit anti-cofilin (1:1,000, Cell Signalling) or rabbit anti-α-tubulin (1 μg/ml, AbCAM), washed and incubated for 1 h at 20–24 °C with horseradish peroxidase (HRP)-conjugated goat anti-rabbit (1:20,000, BioRad). Membranes were washed and incubated for 5 min with chemiluminescent substrate (Pierce) before exposure to film. Band densitometry was performed using Quantity One 4.5.0 software (BioRad).

Two-photon laser scanning microscopy and image analysis. Neurons were imaged with custom-built two-photon laser scanning microscopes[49] with an excitation wavelength of 910 nm. Images of transfected pyramidal neurons were acquired at 0.8× zoom (image field, 300 × 270 μm), whereas spiny regions of basal and apical dendrites were imaged at 5× magnification (image field, 42 × 42 μm). Optical sections were taken at 1.0-μm spacing. Spine density, length and width, as well as soma size, were measured manually using custom software[50] by observers who were blind to genotype. Spine lengths were measured from the junction with the dendritic shaft to the tip. To determine head width and primary dendrite thickness, the fluorescence was measured in a line across each structure and the width of the distribution where fluorescent intensity fell to 30% of maximum was calculated. Measurements performed on 100-nm diameter yellow-green fluorescent microspheres (FluorSpheres, Molecular Probes) indicated that the point-spread function placed a lower limit on measurable widths of 550 nm. The apparent width is the convolution of the true fluorescence distribution and point-spread function of the microscope and has a lower limit of ~550 nm. Therefore, the summaries of spine head widths are plotted from this lower bound. Soma cross-sectional area was measured in the maximum intensity projection of a low-power image stack by counting the number of pixels within an outline drawn around the soma. Proximal dendrites of $Tsc1^{C/C}$ control and Cre-expressing neurons were of similar thickness (control, 1.26 ± 0.1 μm; Cre, 1.49 ± 0.1 μm; $n = 9$–13 cells).

Electrophysiology. Hippocampal slice cultures from $Tsc1^{C/C}$ mice were placed in a recording chamber perfused with artificial cerebrospinal fluid (ACSF) containing 127 mM NaCl, 25 mM $NaHCO_3$, 1.25 mM Na_2HPO_4, 2.5 mM KCl, 2 mM $CaCl_2$, 1 mM $MgCl_2$, 25 mM glucose and saturated with 95% O_2, 5% CO_2 at 20–24 °C. Whole-cell voltage-clamp recordings were obtained using an Axopatch 200B amplifier (Axon Instruments) from Cre-transfected pyramidal neurons (green fluorescence and visible gold particle in soma) and

untransfected neighbors at 10–12 DPT and 18–20 DPT. Transfection with GFP alone had no effect on membrane properties (data not shown).

Borosilicate glass pipettes (3–5 MΩ tip resistance; Warner Instruments Inc.) were filled with 120 mM cesium methane-sulfonate, 10 mM HEPES, 10 mM EGTA, 4 mM $MgCl_2$, 0.4 mM NaGTP, 4 mM MgATP, 10 mM phosphocreatine and 0.02 mM Alexa Fluor-594 (Molecular Probes) at a pH of 7.3 (290 mOsm). Bicuculline (20 μM, Tocris) was added to the bath to block $GABA_A$ receptors in all experiments and tetrodotoxin (1 μM, Sigma) was included to block sodium channels for mEPSC recordings. Series resistance (8–19 MΩ, <20 MΩ for inclusion in data set), input resistance and membrane capacitance were monitored online. mEPSC frequency and amplitude were analyzed in Igor Pro (Wavemetrics) using custom software. EPSCs were evoked at 0.125 Hz with a bipolar electrode placed in the stratum radiatum 250–350 μm from the soma. The AMPAR/NMDAR current ratio was calculated from the ratio of the EPSC peak amplitude at –60 mV to the current at +40 mV 100 ms after the peak. To measure PPF, paired stimuli at an interpulse interval of 50 ms were delivered and the ratio of peak amplitudes of the EPSCs was calculated.

Statistics. Statistical significance was tested by analysis of variance (ANOVA) with, when appropriate, a Tukey-Kramer correction for multiple pairwise comparisons in Matlab (Mathworks) or Microsoft Excel. Distributions of mEPSC amplitudes and immunostaining intensities were compared using Kolmogorov-Smirnov tests. Band intensities of western blots were compared with paired *t*-tests. Summary data is presented as mean ± standard error of the mean (s.e.m.).

Note: Supplementary information is available on the Nature Neuroscience website.

ACKNOWLEDGMENTS

We thank members of the Sabatini lab, D. Schmucker and D. Sabatini for comments on the manuscript; E. Hong, A. Carter and R. Witt for technical assistance and advice; and K. Mizuno, A. Minden, S. Dymecki, E. Henske, V. Ramesh, L. Cantley and Y. Shi for the gift of reagents. This work was supported by the US National Institutes of Health (5T32 NS07484) (to V.A.A.), a Burroughs Wellcome Fund Career Award, the Searle Scholars Fund, the Giovanni Armenise Foundation, the Smith Family Foundation and the US Department of Defense (TS030004).

COMPETING INTERESTS STATEMENT

The authors declare that they have no competing financial interests.

Published online at http://www.nature.com/natureneuroscience/
Reprints and permissions information is available online at http://npg.nature.com/reprintsandpermissions/

1. Gomez, M.R., Sampson, J.R. & Whittemore, V.H. (eds.) *Tuberous Sclerosis Complex* (Oxford Univ. Press, New York, 1999).
2. Ito, N. & Rubin, G.M. Gigas, a *Drosophila* homolog of tuberous sclerosis gene product-2, regulates the cell cycle. *Cell* **96**, 529–539 (1999).
3. Potter, C.J., Huang, H. & Xu, T. *Drosophila* Tsc1 functions with Tsc2 to antagonize insulin signaling in regulating cell growth, cell proliferation, and organ size. *Cell* **105**, 357–368 (2001).
4. Tapon, N., Ito, N., Dickson, B.J., Treisman, J.E. & Hariharan, I.K. The *Drosophila* tuberous sclerosis complex gene homologs restrict cell growth and cell proliferation. *Cell* **105**, 345–355 (2001).
5. Gao, X. & Pan, D. TSC1 and TSC2 tumor suppressors antagonize insulin signaling in cell growth. *Genes Dev.* **15**, 1383–1392 (2001).
6. Potter, C.J., Pedraza, L.G. & Xu, T. Akt regulates growth by directly phosphorylating Tsc2. *Nat. Cell Biol.* **4**, 658–665 (2002).
7. Manning, B.D., Tee, A.R., Logsdon, M.N., Blenis, J. & Cantley, L.C. Identification of the tuberous sclerosis complex-2 tumor suppressor gene product tuberin as a target of the phosphoinositide 3-kinase/akt pathway. *Mol. Cell* **10**, 151–162 (2002).
8. Inoki, K., Li, Y., Zhu, T., Wu, J. & Guan, K.L. TSC2 is phosphorylated and inhibited by Akt and suppresses mTOR signalling. *Nat. Cell Biol.* **4**, 648–657 (2002).
9. Stocker, H. *et al.* Rheb is an essential regulator of S6K in controlling cell growth in *Drosophila*. *Nat. Cell Biol.* **5**, 559–565 (2003).
10. Garami, A. *et al.* Insulin activation of Rheb, a mediator of mTOR/S6K/4E-BP signaling, is inhibited by TSC1 and 2. *Mol. Cell* **11**, 1457–1466 (2003).
11. Hay, N. & Sonenberg, N. Upstream and downstream of mTOR. *Genes Dev.* **18**, 1926–1945 (2004).
12. Sepp, T., Yates, J.R. & Green, A.J. Loss of heterozygosity in tuberous sclerosis hamartomas. *J. Med. Genet.* **33**, 962–964 (1996).
13. Ramesh, V. Aspects of tuberous sclerosis complex (TSC) protein function in the brain. *Biochem. Soc. Trans.* **31**, 579–583 (2003).
14. Dijkhuizen, P.A. & Ghosh, A. BDNF regulates primary dendrite formation in cortical neurons via the PI3-kinase and MAP kinase signaling pathways. *J. Neurobiol.* **62**, 278–288 (2005).
15. Tang, S.J. *et al.* A rapamycin-sensitive signaling pathway contributes to long-term synaptic plasticity in the hippocampus. *Proc. Natl. Acad. Sci. USA* **99**, 467–472 (2002).
16. Hou, L. & Klann, E. Activation of the phosphoinositide 3-kinase-Akt-mammalian target of rapamycin signaling pathway is required for metabotropic glutamate receptor-dependent long-term depression. *J. Neurosci.* **24**, 6352–6361 (2004).
17. Huber, K.M., Kayser, M.S. & Bear, M.F. Role for rapid dendritic protein synthesis in hippocampal mGluR-dependent long-term depression. *Science* **288**, 1254–1257 (2000).
18. Uhlmann, E.J. *et al.* Astrocyte-specific TSC1 conditional knockout mice exhibit abnormal neuronal organization and seizures. *Ann. Neurol.* **52**, 285–296 (2002).
19. Kohn, A.D. *et al.* Construction and characterization of a conditionally active version of the serine/threonine kinase Akt. *J. Biol. Chem.* **273**, 11937–11943 (1998).
20. Meng, Y., Zhang, Y., Tregoubov, V., Falls, D.L. & Jia, Z. Regulation of spine morphology and synaptic function by LIMK and the actin cytoskeleton. *Rev. Neurosci.* **14**, 233–240 (2003).
21. Zhou, Q., Homma, K.J. & Poo, M.M. Shrinkage of dendritic spines associated with long-term depression of hippocampal synapses. *Neuron* **44**, 749–757 (2004).
22. Zhang, H. *et al.* Loss of Tsc1/Tsc2 activates mTOR and disrupts PI3K-Akt signaling through downregulation of PDGFR. *J. Clin. Invest.* **112**, 1223–1233 (2003).
23. Mashimo, J., Maniwa, R., Sugino, H. & Nose, K. Decrease in the expression of a novel TGF beta1-inducible and ras-recision gene, TSC-36, in human cancer cells. *Cancer Lett.* **113**, 213–219 (1997).
24. Tuttle, R.L. *et al.* Regulation of pancreatic beta-cell growth and survival by the serine/threonine protein kinase Akt1/PKBalpha. *Nat. Med.* **7**, 1133–1137 (2001).
25. Verdu, J., Buratovich, M.A., Wilder, E.L. & Birnbaum, M.J. Cell-autonomous regulation of cell and organ growth in *Drosophila* by Akt/PKB. *Nat. Cell Biol.* **1**, 500–506 (1999).
26. Kwon, C.H. *et al.* Pten regulates neuronal soma size: a mouse model of Lhermitte-Duclos disease. *Nat. Genet.* **29**, 404–411 (2001).
27. Backman, S.A. *et al.* Deletion of Pten in mouse brain causes seizures, ataxia and defects in soma size resembling Lhermitte-Duclos disease. *Nat. Genet.* **29**, 396–403 (2001).
28. Dong, J. & Pan, D. Tsc2 is not a critical target of Akt during normal *Drosophila* development. *Genes Dev.* **18**, 2479–2484 (2004).
29. Sarbassov, D.D., Guertin, D.A., Ali, S.M. & Sabatini, D.M. Phosphorylation and regulation of Akt/PKB by the rictor-mTOR complex. *Science* **307**, 1098–1101 (2005).
30. Lamb, R.F. *et al.* The TSC1 tumour suppressor hamartin regulates cell adhesion through ERM proteins and the GTPase Rho. *Nat. Cell Biol.* **2**, 281–287 (2000).
31. Govek, E.E. *et al.* The X-linked mental retardation protein oligophrenin-1 is required for dendritic spine morphogenesis. *Nat. Neurosci.* **7**, 364–372 (2004).
32. Penzes, P. *et al.* The neuronal Rho-GEF Kalirin-7 interacts with PDZ domain-containing proteins and regulates dendritic morphogenesis. *Neuron* **29**, 229–242 (2001).
33. Penzes, P. *et al.* Rapid induction of dendritic spine morphogenesis by trans-synaptic ephrinB-EphB receptor activation of the Rho-GEF kalirin. *Neuron* **37**, 263–274 (2003).
34. Li, Y., Inoki, K., Yeung, R. & Guan, K.L. Regulation of TSC2 by 14–3-3 binding. *J. Biol. Chem.* **277**, 44593–44596 (2002).
35. Hengstschlager, M., Rosner, M., Fountoulakis, M. & Lubec, G. Tuberous sclerosis genes regulate cellular 14–3-3 protein levels. *Biochem. Biophys. Res. Commun.* **312**, 676–683 (2003).
36. Nufer, O. & Hauri, H.P. ER export: call 14–3-3. *Curr. Biol.* **13**, R391–R393 (2003).
37. Gohla, A. & Bokoch, G.M. 14–3-3 regulates actin dynamics by stabilizing phosphorylated cofilin. *Curr. Biol.* **12**, 1704–1710 (2002).
38. Benvenuto, G. *et al.* The tuberous sclerosis-1 (TSC1) gene product hamartin suppresses cell growth and augments the expression of the TSC2 product tuberin by inhibiting its ubiquitination. *Oncogene* **19**, 6306–6316 (2000).
39. Sarbassov, D.D. *et al.* Rictor, a novel binding partner of mTOR, defines a rapamycin-insensitive and raptor-independent pathway that regulates the cytoskeleton. *Curr. Biol.* **14**, 1296–1302 (2004).
40. Arber, S. *et al.* Regulation of actin dynamics through phosphorylation of cofilin by LIM-kinase. *Nature* **393**, 805–809 (1998).
41. Tassabehji, M. *et al.* LIM-kinase deleted in Williams syndrome. *Nat. Genet.* **13**, 272–273 (1996).
42. Hayashi, M.L. *et al.* Altered cortical synaptic morphology and impaired memory consolidation in forebrain-specific dominant-negative PAK transgenic mice. *Neuron* **42**, 773–787 (2004).
43. Bryan, B. *et al.* GEFT, a Rho family guanine nucleotide exchange factor, regulates neurite outgrowth and dendritic spine formation. *J. Biol. Chem.* **279**, 45824–45832 (2004).
44. Meng, Y. *et al.* Abnormal spine morphology and enhanced LTP in LIMK-1 knockout mice. *Neuron* **35**, 121–133 (2002).
45. Chang, H. *et al.* Identification of a cDNA encoding a thiazide-sensitive sodium-chloride cotransporter from the human and its mRNA expression in various tissues. *Biochem. Biophys. Res. Commun.* **223**, 324–328 (1996).
46. Shepherd, C.W., Houser, O.W. & Gomez, M.R. MR findings in tuberous sclerosis complex and correlation with seizure development and mental impairment. *AJNR Am. J. Neuroradiol.* **16**, 149–155 (1995).
47. Boyer, C., Schikorski, T. & Stevens, C.F. Comparison of hippocampal dendritic spines in culture and in brain. *J. Neurosci.* **18**, 5294–5300 (1998).
48. Stoppini, L., Buchs, P.A. & Muller, D.A. A simple method for organotypic cultures of nervous tissue. *J. Neurosci. Methods* **37**, 173–182 (1991).
49. Carter, A.G. & Sabatini, B.L. State dependent calcium signaling in dendritic spines of striatal medium spiny neurons. *Neuron* (2004).
50. Trachtenberg, J.T. *et al.* Long-term *in vivo* imaging of experience-dependent synaptic plasticity in adult cortex. *Nature* **420**, 788–794 (2002).